

Simulation of Patient-Specific Deformable Ultrasound Imaging in Real Time

Mafalda Camara^(✉), Erik Mayer, Ara Darzi, and Philip Pratt

Department of Surgery and Cancer, Imperial College, London, UK
`m.camara15@imperial.ac.uk`

Abstract. Intraoperative ultrasound is an imaging modality frequently used to provide delineation of tissue boundaries. This paper proposes a simulation platform that enables rehearsal of patient-specific deformable ultrasound scanning in real-time, using preoperative CT as the data source. The simulation platform was implemented within the GPU-accelerated NVIDIA FleX position-based dynamics framework. The high-resolution particle model is used to deform both surface and volume meshes. The latter is used to compute the barycentric coordinates of each simulated ultrasound image pixel in the surrounding volume, which is then mapped back to the original undeformed CT volume. To validate the computation of simulated ultrasound images, a kidney phantom with an embedded tumour was CT-scanned in the rest position and at five different levels of probe-induced deformation. Measures of normalised cross-correlation and similarity between features were adopted to compare pairs of simulated and ground truth images. The accurate results demonstrate the potential of this approach for clinical translation.

1 Introduction

Intraoperative imaging has been used for navigation in robotic surgical procedures as a mean to compensate for the limited access, narrowed field-of-view and lack of tactile feedback. In the context of robot-assisted partial nephrectomy (RAPN), intraoperative ultrasound (US) facilitates delineation of the tumour's borders, potentially improves the tumour dissection and minimises the risk of positive margins. The benefit of using such an imaging modality associated with the challenge of acquiring and understanding the data, has encouraged the development of simulation-based environments. Depending on the specific application of the simulator, different features are desired, from real time performance, use of patient-specific data, a biomechanical model to account for deformation and acoustic imaging features. Regarding the use of patient-specific data, by resorting to the GPU and the use of CT volumes, Reichl et al. [1] achieved realistic US images and acoustic features in real time. The similar principle of using imaging volumes and wave propagation techniques has been adopted by Shams et al. [2] and Salehi et al. [3]. The former results in accurate and realistic modelling of acoustic phenomena while using patient-specific data. However, deformation caused by external forces were not integrated into the simulations. Alternatively,

some effort has been focused on compensating for deformation. Pheiffer et al. [4] defined a framework for correcting non-rigid tissue compression induced by the probe in US scanning, to allow for a more accurate volume estimation to be used in image guidance. Flach et al. [5] used a FEM model around the contact areas and the known probe geometry to provide an accurate undeformed 3D volume. Similar work was developed by Goksel et al. [6] to simulate B-mode images of deformable tissue. These techniques depend on the use of a priori known 3D US volumes, commonly unavailable in the context of RAPN. Techniques combining 3D volumes and biomechanical modelling have been adopted to address simultaneously deformation and the use of patient-specific data. Selmi et al. [7] developed a method for realistic 3D deformable US image generation in real time. A biomechanical model was combined with a 3D elastic texture in order to re-slice the patient's volume to achieve deformable US images. Bürger et al. [8] developed an US simulator for medical education based on a convolution ray-tracing approach and a deformable mesh model. Morin et al. [9] simulated US imaging for breast cancer. MRI volumes in combination with a biomechanical model provided the means to simulate realistic US imaging.

The framework adopted in this paper combines the use of a biomechanical model and a 3D preoperative volume to simulate deformable US images interactively. This biomechanical model was previously implemented and validated for a patient-specific surgical simulator, as described in Camara et al. [10]. The focus of the work is not on modelling realistic US images but rather in providing an accurate simulation platform that ultimately provides the user with the opportunity to rehearse scanning with patient-specific data. Additionally, it can act as a validation context for manually-operated 3D tumour acquisition and reconstruction, and to assist further with the automation of intraoperative scanning protocols. The novel aspect in this paper lays on the deformation method implemented for a patient-specific simulation in real time, associated with a straightforward data preparation that enables a facilitated translation into clinical practice.

2 Methods

2.1 Development of a Partial Nephrectomy Phantom

A kidney phantom with embedded tumour was developed in a methodology similar to the one used by Hughes-Hallett [11]. Polyvinyl alcohol (PVA), a polymer that presents similar tensile strength and elasticity to tissue, can be used as a surrogate for soft tissue organs. A 10% PVA by weight concentration solution was used. Regarding mimicking tissue biomechanics, by subjecting the solution to a certain number of freeze-defrost cycles, one can change the material rigidity. A tumour is often stiffer and less elastic when compared to the surrounding renal parenchyma. Therefore, the tumour was subjected to an initial cycle and the overall phantom to an extra cycle to create realistic kidney properties. With respect to CT imaging the phantom, there was a need to clearly differentiate the boundary between tumour and kidney parenchyma. The tumour was enveloped

in a thin layer of dense putty, as it presents an increased radiographic attenuation coefficient and allowed the boundary to be identified. A 3D-printed non-diseased kidney was used as the mould for phantom. The tumour mould was a simple spherical mould with diameter of 2.3 cm.

2.2 Experimental Setup

A rig designed in SolidEdge and 3D-printed with polyamide (Materialise), was used to induce deformation. The rig was composed of a platform designed to support the phantom and a movable structure which represents an US probe. Five different levels of deformation were used (total of 14.6 mm), each inducing approximately a 2.5 mm increment. The bottom part of the kidney mould was used to act as boundary conditions. The combination of mould and kidney was placed within the rig and the movable structure varied its position to desired locations for each set of acquired CT scans. CT images were acquired with a GE Innova 4100 scanner. Initially, the entire setup was CT scanned for no applied deformation. It was always assured that the US probe was positioned as if scanning part of the tumour and that the probe was rigidly fixed. This procedure was continued for the different levels of deformation, by moving the probe to the subsequent level of deformation and CT scanning the setup. The entire setup is showed in Fig. 1(a).

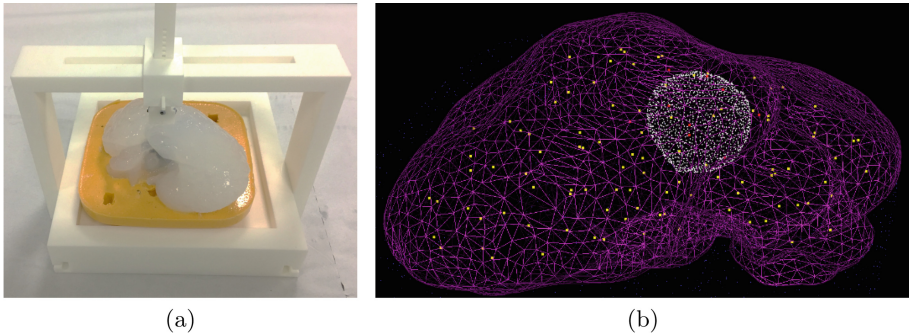


Fig. 1. (a) Deformation rig with phantom and support, placed on the CT scanner table. (b) Cluster distribution within tumour (red) and kidney (yellow) meshes. (Color figure online)

2.3 Simulation Platform and Biomechanical Model

The simulation platform was implemented within the GPU-accelerated NVIDIA FleX position-based dynamics framework [12], in a manner similar to that reported in Camara et al. [10]. All structures of interest, i.e. the kidney, tumour, support mesh and structure representing the US probe, were segmented from the 3DCT scans using ITK-SNAP and exported as surface mesh files. Kidney

and tumour meshes were imported to MeshLab, whereby smoothed (using the volume-preserving HC Laplacian smoothing algorithm) and decimated (with the quadratic edge collapse decimation algorithm). The FleX framework supports different forms of modelling structure and collision geometries. The tumour mesh was modelled as a triangular mesh, solely used for analysis, whereas the kidney, which embeds the tumour region, was modelled as a combination of particles. These particles were distributed and clustered together into shape-matching clusters, assuming two different values of stiffness coefficients. For all the clusters where centroids were found within the tumour mesh boundaries, the cluster stiffness coefficient modelled the tumour deformation, whereas the remaining clusters were assigned to a different stiffness coefficient to model the kidney deformation. This assured that the approximate regions of kidney and tumour were modelled as different structures. The support structure was represented as a static triangular mesh and used as boundary conditions for the kidney model. The ultrasound transducer (Aloka UST-533) was approximated as a cuboid and modelled as a dynamic convex mesh. Both the vertices of the tumour mesh and triangular mesh representing the kidney surface were defined in accordance with local particle positions through a weighted matrix bending technique, often referred as ‘skinning’ [13]. Therefore, the structures attached to the particle system deformed in terms of the manipulated kidney parenchyma. The representation of clusters, kidney and tumour surface meshes are showed in Fig. 1(b).

2.4 Ultrasound Simulation

The deformable US scans were simulated by using the same ‘skinning’ technique. A tetrahedral mesh for the kidney was computed with Gmsh and imported into the simulation. This mesh was embedded within the particle system and deformed in accordance with its displacements. A planar discretisation, i.e. a grid of 1×2 cm with a resolution of 0.25 mm, was registered to the US probe to display the deformable slice, by means of an efficient interpolation method that mapped the simulated ultrasound pixels to the undeformed voxels in the respective CT volume. Each ultrasound image pixel was expressed by barycentric coordinates in terms of the tetrahedral mesh vertices, and then mapped back to the voxels of the respective undeformed CT volume. For each image pixel $\mathbf{p} = [x \ y \ z]^T$, its 3D position within a tetrahedral element t , can be expressed as

$$\mathbf{p} = \sum_{i=0}^3 \lambda_i \mathbf{r}_i \quad \text{with} \quad \sum_{i=0}^3 \lambda_i = 1, \lambda_i \geq 0 \quad (1)$$

where λ_i are the barycentric coordinates in terms of the element corners $\mathbf{r}_i = [x_i \ y_i \ z_i]^T$, which represent the deformed ‘skinned’ vertices. Rearranging Eq. 1 and expressing it in a matrix form, results in

$$\mathbf{T}\boldsymbol{\lambda} = \mathbf{p} - \mathbf{r}_3 \quad (2)$$

where the matrix \mathbf{T} and the array $\boldsymbol{\lambda}$ are defined as

$$\mathbf{T} = \begin{bmatrix} x_0 - x_3 & x_1 - x_3 & x_2 - x_3 \\ y_0 - y_3 & y_1 - y_3 & y_2 - y_3 \\ z_0 - z_3 & z_1 - z_3 & z_2 - z_3 \end{bmatrix}, \boldsymbol{\lambda} = [\lambda_1 \ \lambda_2 \ \lambda_3]^T$$

The barycentric coordinates can be found solving Eq. 2 for $\boldsymbol{\lambda}$,

$$\boldsymbol{\lambda} = \mathbf{T}^{-1}(\mathbf{p} - \mathbf{r}_3) \quad (3)$$

Finally, to recover the pixel texture coordinates from the undeformed voxels, as pixel \mathbf{p} is defined by the same barycentric coordinates in the original configuration and the deformed state, one needs to solve the following equation,

$$\mathbf{p} = \mathbf{T}^0 \boldsymbol{\lambda} + \mathbf{r}_3^0 \quad (4)$$

where \mathbf{T}^0 and \mathbf{r}_i^0 describe the undeformed state and are expressed as

$$\mathbf{T}^0 = \begin{bmatrix} x_0^0 - x_3^0 & x_1^0 - x_3^0 & x_2^0 - x_3^0 \\ y_0^0 - y_3^0 & y_1^0 - y_3^0 & y_2^0 - y_3^0 \\ z_0^0 - z_3^0 & z_1^0 - z_3^0 & z_2^0 - z_3^0 \end{bmatrix}, \mathbf{r}_i^0 = [x_i^0 \ y_i^0 \ z_i^0]^T$$

To compare the simulated slices with the respective ground truth images, the location of pixels within the grid was registered to the respective CT volume and saved into an image. The process was repeated for all levels of deformation. The mapping technique to estimate both the simulated and ground truth images is similar, but where simulated slices map the grid to the undeformed volume by means of skinning the particle system, the ground truth slices are obtained by mapping the grid to the volume respective of each level of deformation.

2.5 Calibration

An estimation of parameters to model soft tissue deformation of the porcine kidney was achieved in Camara et al. [10], but a calibration is still necessary as the model used here is a phantom presenting different material properties and hence, different deformation behaviour. Therefore, a calibration was performed to determine the framework parameters that allowed for the most realistic deformation modelling and validation of US simulation. A simple two-dimensional search was used to determine the ideal cluster stiffness coefficient of the general kidney parenchyma, for a given particle radius. The stiffness coefficient for clusters embedded within the tumour boundary was defined as 0.95, as the tumour is known to be stiffer than the surrounding kidney parenchyma, for this specific phantom. The particle radius was permitted in the range [2.2, 2.5, 5.7, 3.0, 3.3] mm and the remaining clusters with a stiffness coefficient in a range [0,1]. The simulation sub-steps and sub-steps iterations were defined as 3 and 9, respectively. The metric undergoing minimisation was the difference, in percentage, of the average count of tumour and kidney pixels between the simulated and the ground truth slices.

3 Results

The metric undergoing minimisation achieved a minimum of 4.5%, across all levels of deformation, for a cluster stiffness coefficient of 0.6 and radius of 2.2 mm. The resulting US image for each level of deformation, against the ground truth, is visible in Fig. 2. Normalised cross-correlation and the difference in approximate distances of the upper and lower extends of boundaries between the simulated and ground truth tumour meshes, are showed in Fig. 3. Absolute distance between the same meshes is showed in Fig. 4. For no deformation, these meshes resemble in volume by 97% compared to the 79% achieved for the 5th level of deformation.

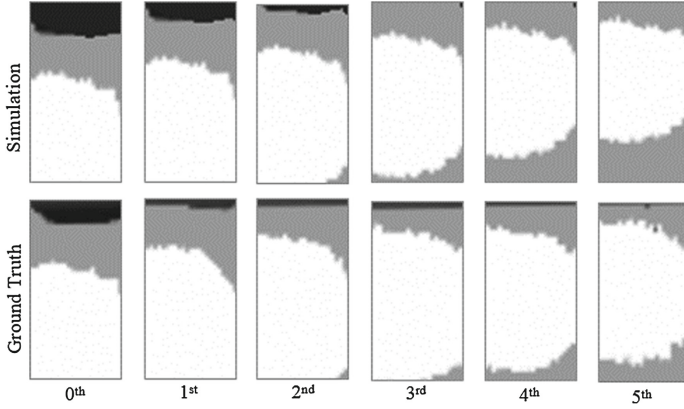


Fig. 2. US images for the increasing levels of deformation (from left to right), of the simulated (top) and ground truth (bottom) slices. Cluster stiffness coefficient was defined as 0.6 and particle radius as 2.2 mm.

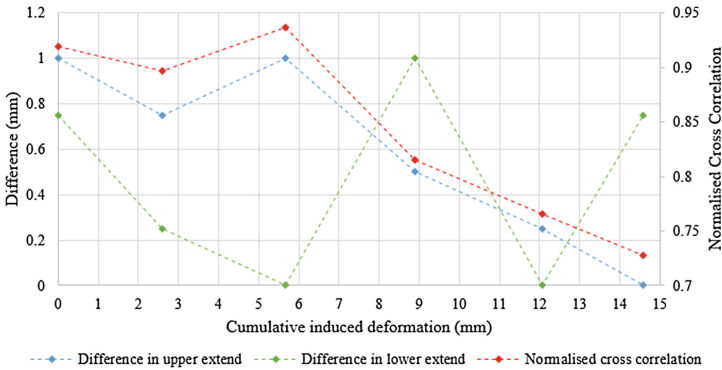


Fig. 3. The left axis represents the difference between the simulated and ground truth slice as a function of the cumulative induced deformation, for the upper and lower extents. The right axis represents the normalised cross-correlation between both images.

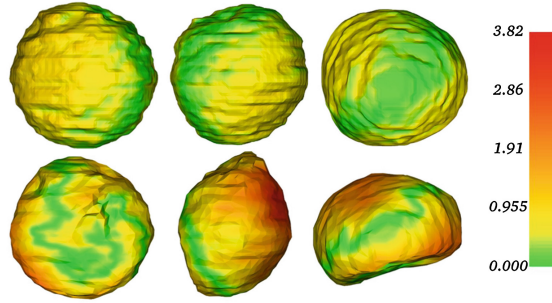


Fig. 4. Representation of the absolute distance (in mm) between the simulated and ground truth tumour meshes. From left to right are represented the anterior, right and inferior views. From top to bottom are represented the 0^{th} and 5^{th} levels of deformation.

4 Discussion and Conclusion

The normalised cross-correlation follows a decreasing trend as the induced deformation increases. The same conclusion is observed in Fig. 2, where the tumour to kidney boundary between the simulated and ground truth images seem to better align for the initial levels of deformation. The tumour meshes in Fig. 4 show similar results, where the pair of meshes presents increasing absolute difference in surface distance for increasing levels of deformation. Regardless of the level of deformation induced by the probe, the difference in the tumour deformation represented in the US slices is smaller than to 1 mm. In the context of an overall displacement of 14.5 mm induced by the US probe, the simulation results in an accurate deformation and visualisation of the US images. The imperfect alignment of the scans and tumour meshes for no applied deformation can only be caused by gravity. Therefore, there is an initial influence on the displacement of particles that was not compensated for throughout the simulation. The use of complex geometries for the phantom and boundary conditions might also influence on the accuracy of the simulation. A three dimensional exhaustive search would have been ideal if accounting for the calibration of the cluster stiffness coefficient for the clusters within the tumour boundaries. Future work will focus on the addition of ultrasound imaging features to improve the realism of the slices. The need for initial gravity compensation will also be addressed. To note that the simulation is patient-specific solely regarding geometry. As described in Miller K. et al. [14], the adoption of patient-specific tissue properties in this family of applications is of secondary importance. Though the simulation uses methodology-based parameters, these can be mapped to real tissue properties in a manner similar to that described in Roberto C. et al. [15].

This paper presents a framework that accurately simulates deformable US slices in real time using patient-specific imaging as source of data. The implemented methodology, which provides a stable and robust real time simulation, coupled with a feasible data preparation, enables a facilitated translation into clinical practice and patient-specific simulation possible on a broader scale.

Acknowledgements. The authors are grateful for the support from the Northwick Park Institute for Medical Research, the Hamlyn Centre for Robotic Surgery and from The Imperial NIHR Biomedical Research Centre (BRC).

References

1. Reichl, T., Passenger, J., Acosta, O., Salvado, O.: Ultrasound goes GPU: real-time simulation using CUDA. In: SPIE Medical Imaging, International Society for Optics and Photonics, p. 726116 (2009)
2. Shams, R., Hartley, R., Navab, N.: Real-time simulation of medical ultrasound from CT images. In: Metaxas, D., Axel, L., Fichtinger, G., Székely, G. (eds.) MICCAI 2008. LNCS, vol. 5242, pp. 734–741. Springer, Heidelberg (2008). doi:[10.1007/978-3-540-85990-1_88](https://doi.org/10.1007/978-3-540-85990-1_88)
3. Salehi, M., Ahmadi, S.-A., Prevost, R., Navab, N., Wein, W.: Patient-specific 3D ultrasound simulation based on convolutional ray-tracing and appearance optimization. In: Navab, N., Hornegger, J., Wells, W.M., Frangi, A.F. (eds.) MICCAI 2015. LNCS, vol. 9350, pp. 510–518. Springer, Cham (2015). doi:[10.1007/978-3-319-24571-3_61](https://doi.org/10.1007/978-3-319-24571-3_61)
4. Pheiffer, T.S., Thompson, R.C., Rucker, D.C., Simpson, A.L., Miga, M.I.: Model-based correction of tissue compression for tracked ultrasound in soft tissue image-guided surgery. *Ultrasound Med. Biol.* **40**(4), 788–803 (2014)
5. Flack, B., Makhinya, M., Goksel, O.: Model-based compensation of tissue deformation during data acquisition for interpolative ultrasound simulation. In: 2016 IEEE 13th International Symposium Biomedical Imaging (ISBI), pp. 502–505 (2016)
6. Goksel, O., Salcudean, S.E.: B-mode ultrasound image simulation in deformable 3-D medium. *IEEE Trans. Med. Imaging* **28**(11), 1657–1669 (2009)
7. Selmi, S.-Y., Promayon, E., Sarrazin, J., Troccaz, J.: 3D interactive ultrasound image deformation for realistic prostate biopsy simulation. In: Bello, F., Cotin, S. (eds.) ISBMS 2014. LNCS, vol. 8789, pp. 122–130. Springer, Cham (2014). doi:[10.1007/978-3-319-12057-7_14](https://doi.org/10.1007/978-3-319-12057-7_14)
8. Bürger, B., Bettinghausen, S., Radle, M., Hesser, J.: Real-time GPU-based ultrasound simulation using deformable mesh models. *IEEE Trans. Med. Imaging* **32**(3), 609–618 (2013)
9. Morin, R., Eiben, B., Bidaut, L., Hipwell, J., Evans, A., Hawkes, D.J.: 3D ultrasound simulation based on a biomechanical model of prone MRI in breast cancer imaging. In: 2015 IEEE 12th International Symposium Biomedical Imaging (ISBI), pp. 264–267 (2015)
10. Camara, M., Mayer, E., Darzi, A., Pratt, P.: Soft tissue deformation for surgical simulation: a position-based dynamics approach. *Int. J. Comput. Assist. Radiol. Surg.* **11**(6), 919–928 (2016)
11. Hughes-Hallett A.: The image-enhanced operating environment in robot assisted laparoscopic partial nephrectomy. Imperial College London (2016)
12. NVIDIA Gameworks. Nvidia Flex. <https://developer.nvidia.com/flex>
13. Kavan, L.: Part I: direct skinning methods and deformation primitives. In: ACM SIGGRAPH, pp. 1–11 (2014)
14. Miller, K., Lu, J.: On the prospect of patient-specific biomechanics without patient-specific properties of tissues. *J. Mech. Behav. Biomed. Mater.* **27**, 154–166 (2013)
15. Rodero, C., Real, P., Zuñeda, P., Monteagudo, C., Lozano, M., García-Fernández, I.: Characterisation of position based dynamics for elastic materials. In: Proceedings of the XXVI Spanish Computer Graphics Conference, pp. 49–57 (2016)

Imaging for Patient-Customized Simulations and
Systems for Point-of-Care Ultrasound
International Workshops, BIVPCS 2017 and POCUS
2017, Held in Conjunction with MICCAI 2017, Québec
City, QC, Canada, September 14, 2017, Proceedings
Cardoso, J.; Arbel, T.; Tavares, J.M.R.S.; Aylward, S.; Li,
S.; Bector, E.; Fichtinger, G.; Cleary, K.; Freeman, B.;
Kohli, L.; Shipley Kane, D.; Oetgen, M.; Pujol, S. (Eds.)
2017, XV, 164 p. 99 illus., Softcover
ISBN: 978-3-319-67551-0